Electronic Supplementary Information

Experimental

Materials: Sodium molybdate (Na_2MoO_4), lithium perchlorate ($LiClO_4$), thiourea (CH_4N_2S), ammonium chloride (NH_4Cl), salicylic acid ($C_7H_6O_3$), sodium citrate dehydrate ($C_6H_5Na_3O_7 \cdot 2H_2O$), *p*-dimethylaminobenzaldehyde ($C_9H_{11}NO$), sodium nitroferricyanide dihydrate ($C_5FeN_6Na_2O \cdot 2H_2O$), sodium hypochlorite solution (NaClO) and graphite powder were purchased from Aladdin Ltd. (Shanghai, China). Nafion (5 wt%) solution was purchased from Sigma-Aldrich Chemical Reagent Co., Ltd. Hydrochloric acid, nitric acid, sulfuric acid, hydrogen peroxide, hydrazine monohydrate ($N_2H_4 \cdot H_2O$), and ethyl alcohol (C_2H_5OH) were purchased from Kelong chemical Ltd. The ultrapure water used throughout all experiments was purified through a UP system. All reagents were analytical reagent grade without further purification.

Preparation of MoS_2 reduced graphene oxide hybrid: Firstly, GO was synthesized by a modified Hummer's method. Then the GO suspension (30mg) and Na_2MoO_4 (300mg) solution were mixed. The mixed solutions (30 mL) were stirred for 10 minutes. After that, 0.63 g of CH_4N_2S was added and dissolved in the mixture. The resulting mixture was ultrasonicated for 30 min and then transferred to a 50 mL Teflon-lined stainless-steel autoclave for 24 h at 200 °C. The resulting product was collected by centrifugation at 6000rpm about 5 min, and washed with deionized water and absolute ethanol for several times and dried at room temperature under vacuum for 24 h followed by further thermal treatment at 800 °C in an Ar environment for 2 h. It should be noted that GO was translated into rGO in the process of reaction. The resulted composites were denoted as MoS_2-rGO. For comparison, we also synthesized rGO or MoS_2 without the addition of Na_2MoO_4 or GO under the same conditions.

Characterizations: XRD analysis was performed using a LabX XRD-6100 X-ray diffractometer with Cu Kα radiation (λ = 1.5418 Å) at 40 kV and 40 mA. SEM images were collected on a XL30 ESEM FEG scanning electron microscope at an accelerating voltage of 20 kV. The structures of the samples were determined by TEM

images on a HITACHI H-8100 electron microscopy (Hitachi, Tokyo, Japan) operated at 200 kV. XPS measurements were performed on an ESCALABMK II X-ray photoelectron spectrometer using Mg as the exciting source. Raman spectra were obtained by a Renishaw Invia confocal Raman microprobe at 532 nm laser excitation. The absorbance data of spectrophotometer were measured on UV-Vis spectrophotometer. The specific surface area of nitrogen sorption isotherms was performed at -196°C in a Micromeritics Instrument Corporation TriStar II 3020 volumetric adsorption system. The data of ion chromatography were measured on Swiss Wang tong ECO. 1H-NMR measurements were performed on a Bruker Avance III 400 MHz spectrometer and dimethyl sulfoxide-d6 was used as an internal to calibrate the chemical shifts in the spectra.

Electrochemical Measurements: Electrochemical NRR measurements were performed in a two-compartment cell separated by Nafion 211 membrane using a CHI 660E electrochemical analyzer (CH Instruments, Inc.). The electrochemical experiments were carried out with a three-electrode configuration using graphite rod as the counter electrode and Ag/AgCl electrode (saturated KCl) as the reference electrode. The working electrode was a CP with catalysts. In a typical synthesis of electrode, 10 mg of the catalyst was dispersed in 1 mL of alcohol containing Nafion solution (5 wt %), followed by ultrasonic treatment for 30 min to form a homogeneous ink. Then, 10 μL of the ink was loaded onto a carbon paper electrode with area of 1 x 1 cm^2 and dried under ambient condition, the catalyst loading mass is 0.1 mg. The potentials reported in this work were converted to RHE scale via calibration with the following equation: E (vs. RHE) = E (vs. Ag/AgCl) + 0.256 V and the presented current density was normalized to the geometric surface area. For electrochemical N_2 reduction, chrono-amperometry tests were conducted in N_2-saturated 0.1 M $LiClO_4$ solution ($LiClO_4$ electrolyte was purged with N_2 for 30 min before measurement).

Determination of NH_3: Concentration of produced NH_3 was spectrophotometrically determined by the indophenol blue method.[1] Typically, 2 mL electrolyte was taken from the cathodic chamber, and then 2 mL of 1 M NaOH solution containing 5% salicylic acid and 5% sodium citrate was added into this solution. Subsequently, 1 mL

of 0.05 M NaClO and 0.2 mL of 1% $C_5FeN_6Na_2O \cdot 2H_2O$ were add into the above solution. After standing at room temperature for 1 h, UV-Vis absorption spectrum was measured at a wavelength of 655 nm. The concentration-absorbance curves were calibrated using standard NH_3 solution with a serious of concentrations. The fitting curve ($y = 0.2377x + 0.02499$, $R^2 = 0.997$) shows good linear relation of absorbance value with NH_3 concentration by three times independent calibrations.

Determination of hydrazine (N_2H_4*)*: N_2H_4 presented in the electrolyte was estimated by the method of Watt and Chrisp.[2] A mixed solution of 5.99 g $C_9H_{11}NO$, 30 mL HCl and 300 mL ethanol was used as a color reagent. Calibration curve was plotted as follow: firstly, preparing a series of reference solutions; secondly, adding 5 mL above prepared color reagent and stirring 20 min at room temperature; finally, the absorbance of the resulting solution was measured at 455 nm, and the yields of N_2H_4 were estimated from a standard curve using 5 mL residual electrolyte and 5 mL color reagent. Absolute calibration of this method was achieved using $N_2H_4 \cdot H_2O$ solutions of known concentration as standards, and the fitting curve shows good linear relation of absorbance with $N_2H_4 \cdot H_2O$ concentration ($y = 0.6166x + 0.0398$, $R^2 = 0.997$) by three times independent calibrations

FE determination: The FE for N_2 reduction was defined as the amount of electric charge used for synthesizing NH_3 divided the total charge passed through the electrodes during the electrolysis. The total amount of NH_3 produced was measured using colorimetric methods. Assuming three electrons were needed to produce one NH_3 molecule, the FE could be calculated as follows:

$$FE = 3 \times F \times [NH_4^+] \times V / (17 \times Q)$$

The rate of NH_3 formation was calculated using the following equation:

$$\text{Ammonia formation rate} = [NH_4^+] \times V / (m \times t)$$

Where F is the Faraday constant, C_{NH_3} is the measured NH_3 concentration, V is the volume of the $LiClO_4$ electrolyte for NH_3 collection, t is the reduction time and $m_{cat.}$ is the catalyst mass.

Computational Details: All DFT calculations were carried out using the Vienna Ab

initio Simulation Package (VASP).[3,4] The interaction between valence electron and ion core is described by the projector-augmented wave method (PAW).[5] Generalized gradient approximation (GGA) with Perdew−Burke−Ernzerhof (PBE) functional[6] is applied to describe the electron exchange-correlation. For the MoS_2/graphene systems, theoretical studies have been reported to understand the structural and electrical properties.[7−10] Recently studies have shown that the edge of MoS_2 is electrocatalytically active site and the Mo-edge plays the key role for N_2 reduction reaction.[11] In order to understand the effect of graphene on the N_2 reduction on MoS_2 edge, the structure of MoS_2-rGO was constructed. The reported band structure of MoS_2-rGO showed that enormous bands appear at the Fermi level and the enhanced electron transfer mainly caused by the MoS_2 edges,[7] which is responsible for the enhanced catalytic activity observed in our experiment.

Herein, we mainly considered the N_2 reduction process on the MoS_2-rGO structure. The (5×5) graphene−(4×4) MoS_2 was adopted to minimize the lattice mismatch of the sample. The width of MoS_2 is about 10 Å and the distance between the MoS_2 with its periodic image is 15.59 Å, which is large enough to avoid artificial interactions displayed in Figure A. The van der Waals (vdW) correction by Grimme's DFT-D2 method[12] is further added to describe the non-bonded interaction between MoS_2 and graphene. The cutoff of kinetic energy was 450 eV and the total energy was converged to less than 10^{-5} eV. The atomic positions were optimized until the force on each atom was less 0.02 eV/Å and dipole corrections in the z direction were considered. In order to improve efficiency, the larger supercell was optimized with the Brillouin zone sampling limited to the gamma point. The vacuum layer of 15 Å thickness was set to avoid the interaction between the periodic images. The Gibbs free energy (G) of a species is calculated by

$$G = E + \mathrm{ZPE} - TS$$

where E is the total energy of adsorbed species from DFT calculations, ZPE and S are the zero-point energy and entropy of a species respectively, and T = 298.15 K. Thermal corrections for gas molecules are from database.[13]

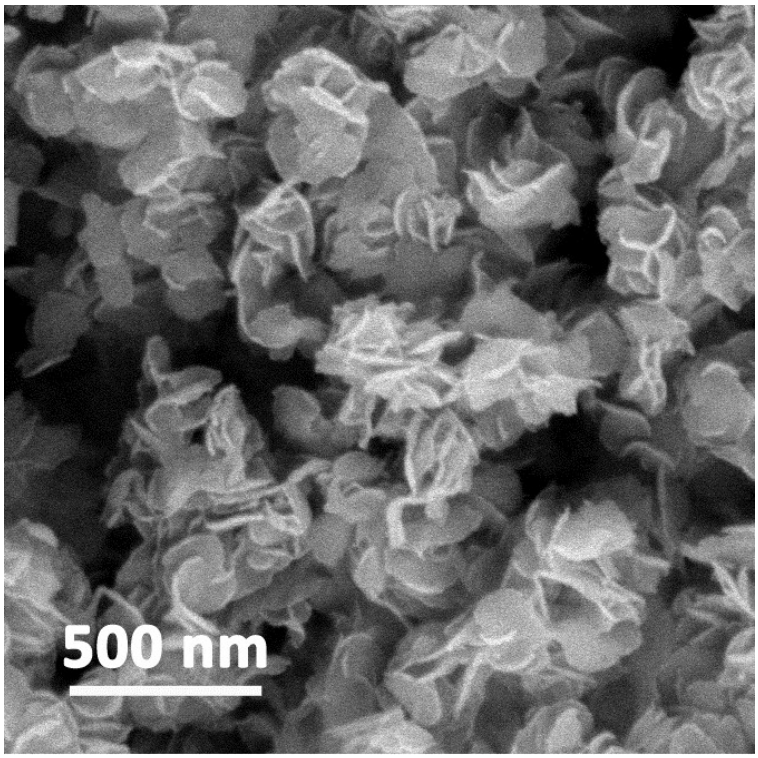

Fig. S1. SEM image of MoS_2.

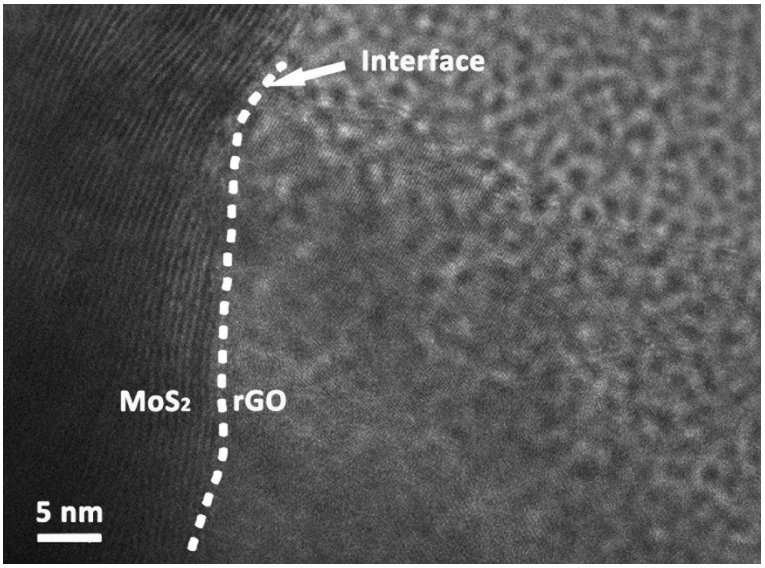

Fig. S2. HRTEM image for MoS_2-rGO hybrid.

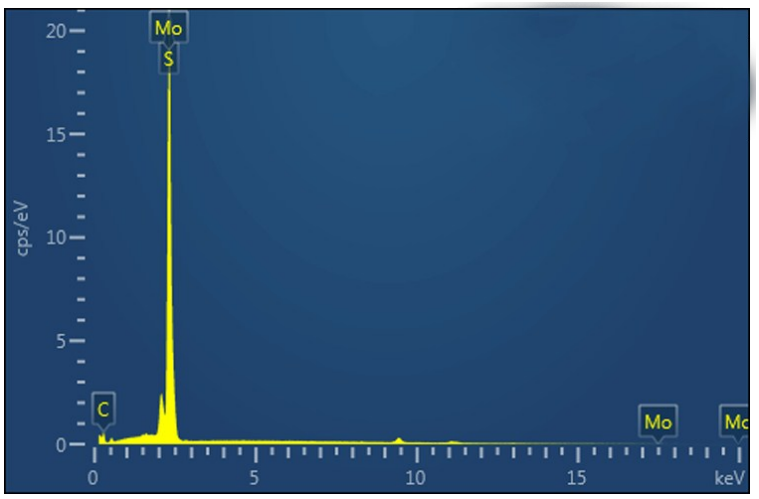

Fig. S3. EDX spectrum of MoS_2-rGO.

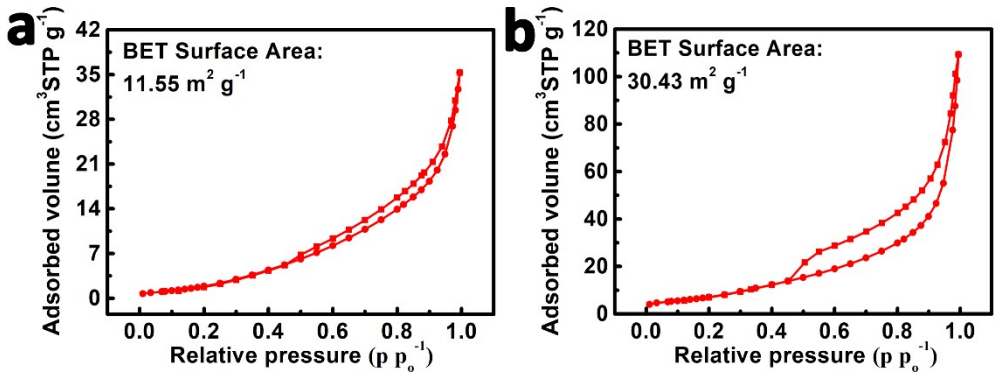

Fig. S4. The N_2 adsorption curve of (a) MoS_2 and (b) MoS_2-rGO.

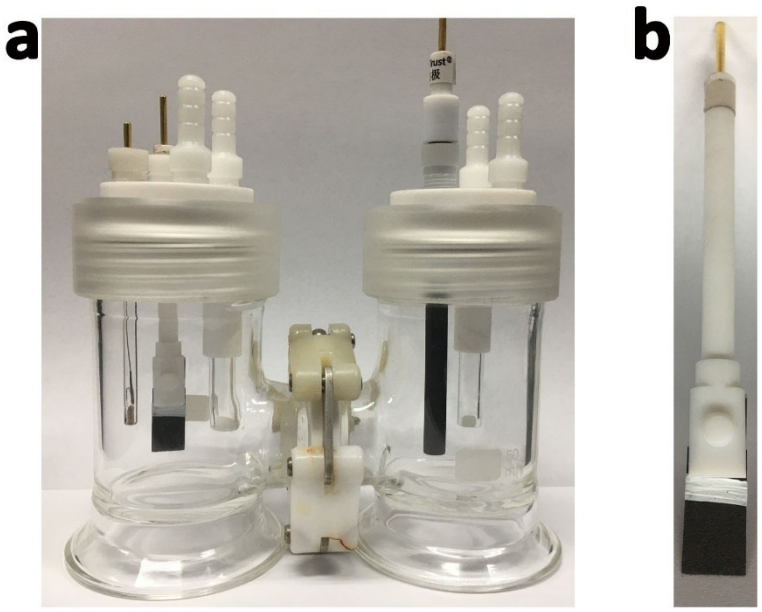

Fig. S5. (a) Optical photograph of the reactor. (b) Optical photograph of the prepared cathode.

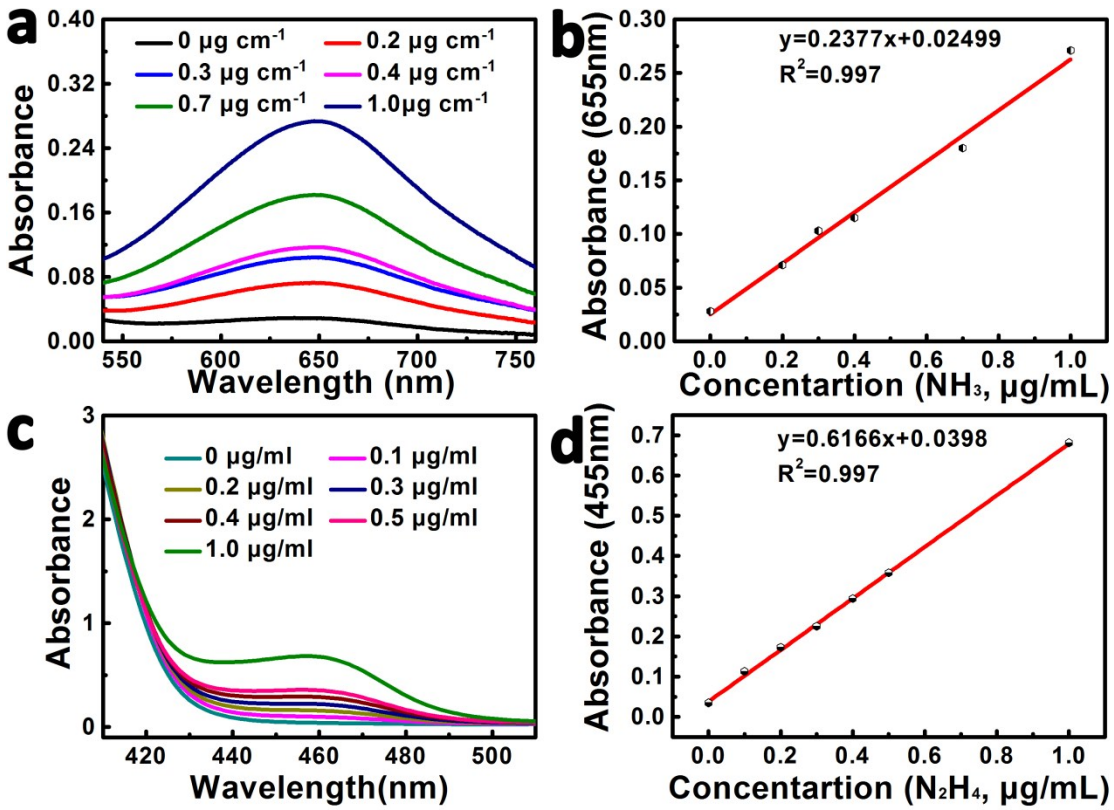

Fig. S6. (a) UV-Vis spectra of indophenol assays with NH_4^+ ions after incubated for 2 h at room temperature. (b) Calibration curve used for estimation of NH_3. (c) UV-Vis absorption spectra of various N_2H_4 concentrations after incubation for 20 min at room temperature. (d) Calibration curve used for calculation of N_2H_4 concentrations.

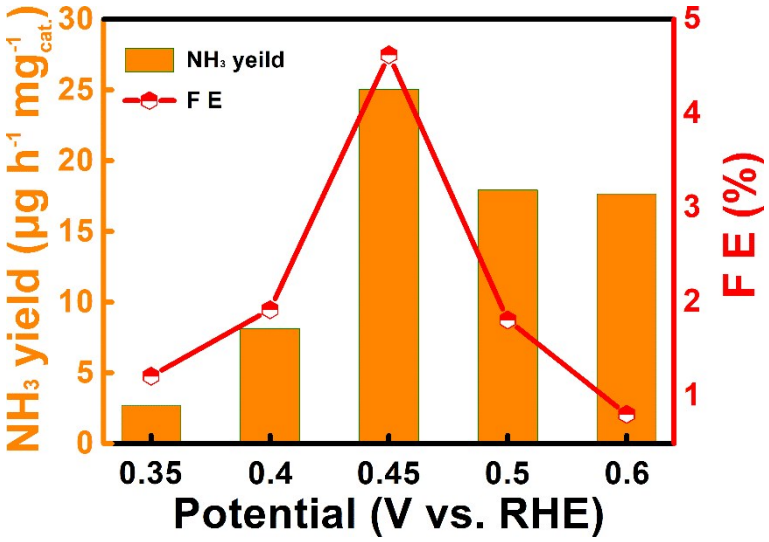

Fig. S7. NH_3 yields and FEs for MoS_2-rGO/CPE at a series of potentials for 2h obtained by ion chromatography.

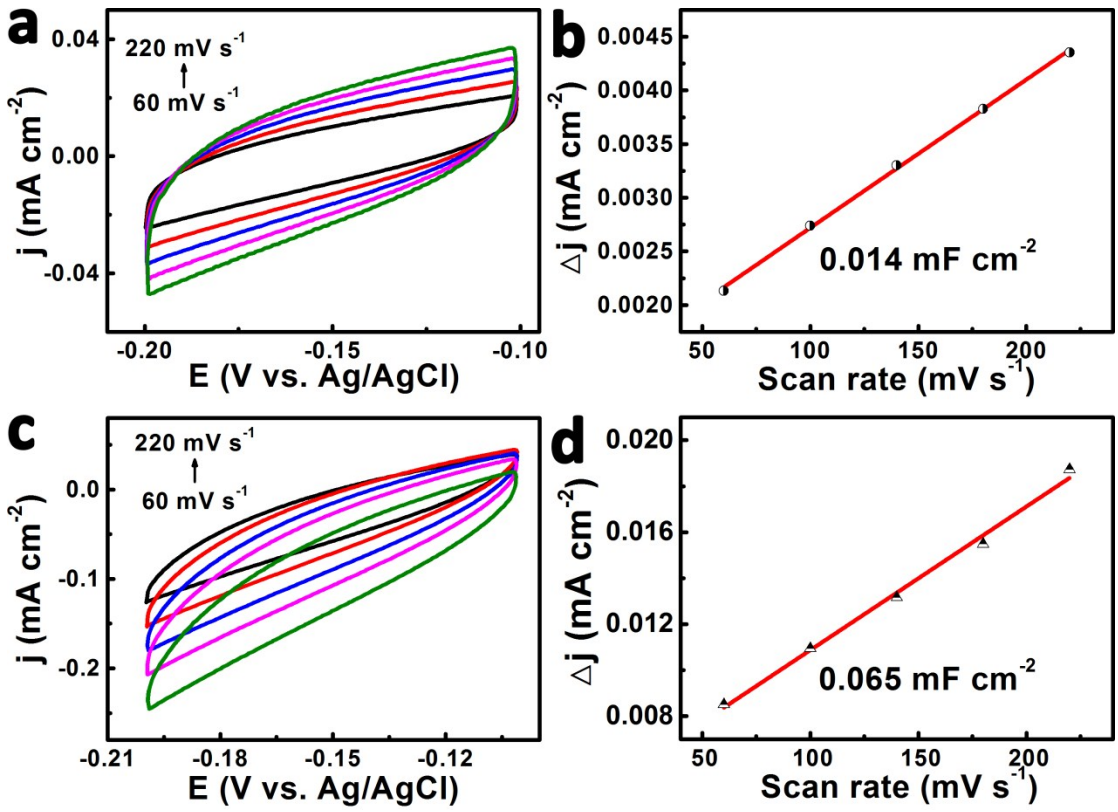

Fig. S8. (a) CVs and (b) capacitive current densities of MoS_2/CPE. (c) CVs and (d) capacitive current densities of MoS_2-rGO/CPE.

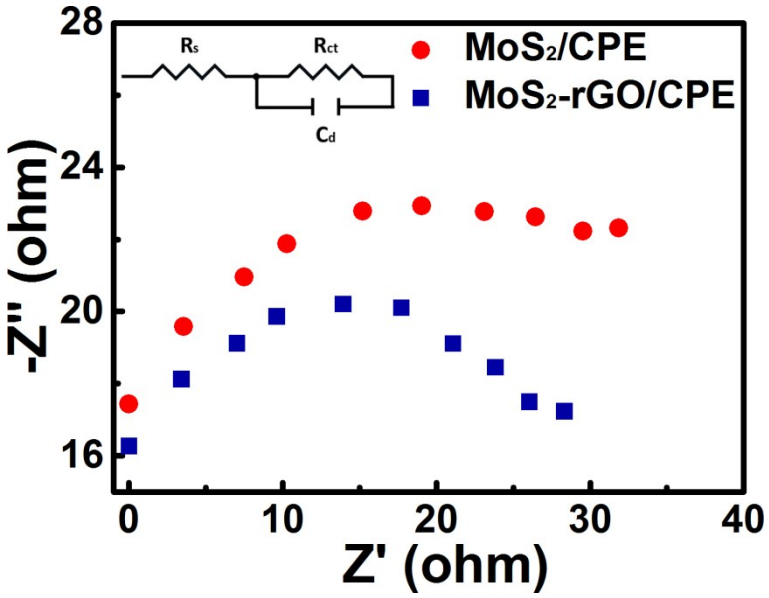

Fig. S9. Nyquist plots of MoS_2-rGO/CPE and MoS_2/CPE.

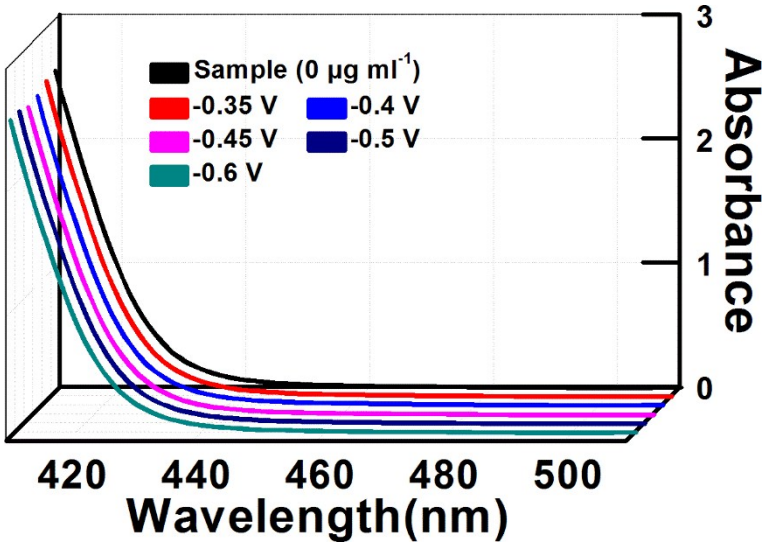

Fig. S10. UV-Vis absorption spectra of the electrolytes estimated by the method of Watt and Chrisp before and after electrolysis in N_2-saturated 0.1 M $LiClO_4$ for MoS_2-rGO/CPE.

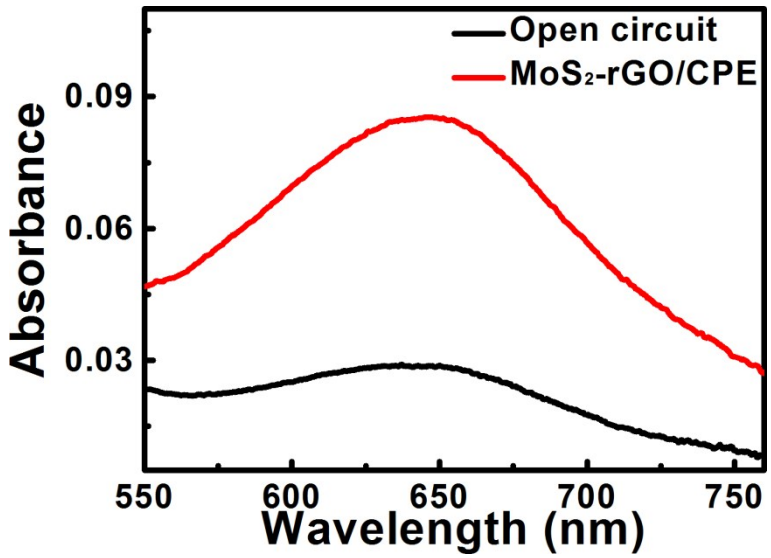

Fig. S11. UV-Vis absorption spectra of the electrolytes stained with indophenol indicator after 2-h electrolysis under different conditions.

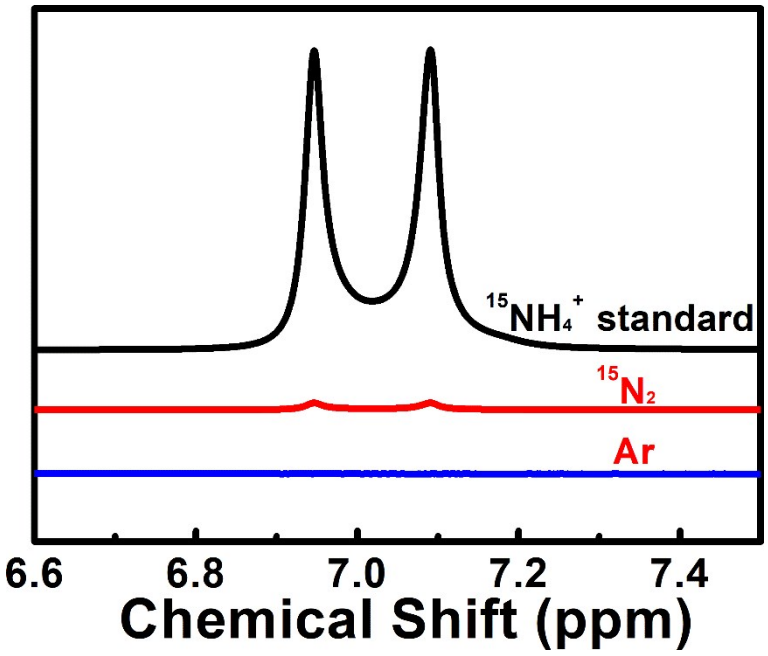

Fig. S12. ^{1}H NMR spectra of $^{15}NH_4^+$ calibration solution, after electrolysis at –0.45 V under $^{15}N_2$ and Ar atmosphere on the MoS_2-rGO/CPE.

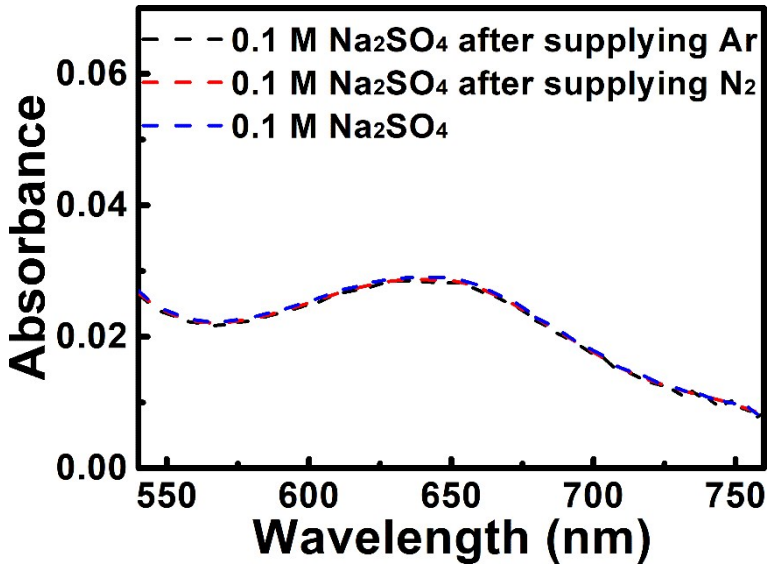

Fig. S13. UV-Vis absorption spectra of the 0.1 M Na_2SO_4 electrolyte stained with indophenol indicator after continuously supplying N_2 or Ar with no applied voltage.

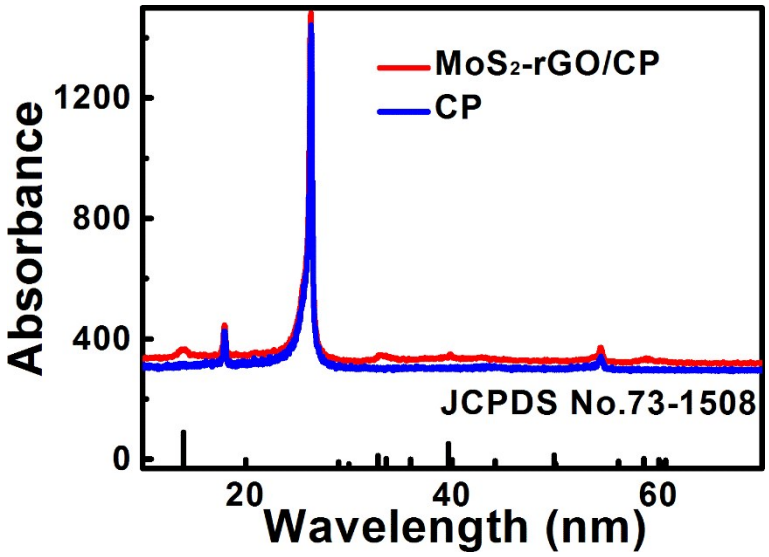

Fig. S14. XRD patterns for CP and MoS_2-rGO/CP after stability test.

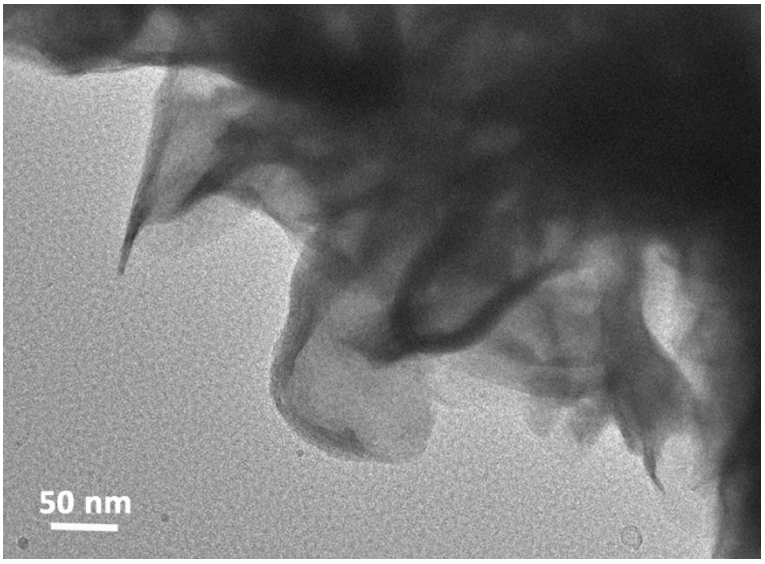

Fig. S15. TEM image for MoS_2-rGO after stability test.

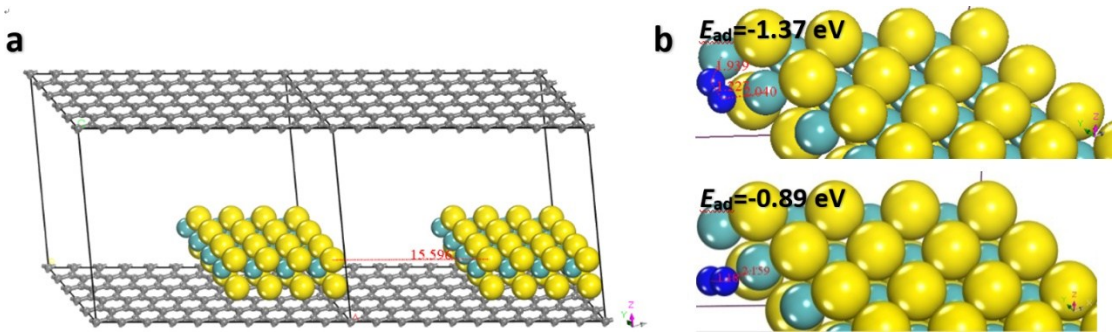

Fig. S16. (Left) Side view of MoS_2-rGO. The green, yellow and grey balls represent Mo, S and C atoms, respectively. (Right) Different N_2 adsorption sites of MoS_2. The blue ball represents N atom.

Table S1. Comparison of electrocatalytic N_2 reduction performance for MoS_2-rGO with other electrocatalysts under ambient conditions.

Catalyst	Electrolyte	NH_3 yield	FE%	Ref.
MoS_2-rGO/CP	**0.1 M $LiClO_4$**	**24.82 μg h^{-1} $mg^{-1}_{cat.}$**	**4.58**	**This work**
$Pd_{0.2}Cu_{0.8}$/rGO	0.1 M KOH	2.8 μg h^{-1} $mg^{-1}_{cat.}$	4.5	14
Au nanorods	0.1 M KOH	1.6 μg h^{-1} cm^{-2}	3.88	15
AuHNCs	0.5 M $LiClO_4$	3.90 μg h^{-1} cm^{-2}	30.2	16
Ag nanosheet	0.1 M HCl	2.83 μg h^{-1} cm^{-2}	4.8	17
Rh	0.1 M KOH	23.88 μg h^{-1} $mg^{-1}_{cat.}$	0.217	18
Pd-Co/CuO	0.1 M KOH	10.04 μg h^{-1} $mg^{-1}_{cat.}$	2.16	19
Pd/C	0.1M PBS	4.5 μg h^{-1} $mg^{-1}_{cat.}$	8.2	20
$Bi_4V_2O_{11}/CeO_2$	0.1 M HCl	23.21 μg h^{-1} $mg^{-1}_{cat.}$	10.16	21
hollow Cr_2O_3 microspheres	0.1 M Na_2SO_4	25.3 μg h^{-1} $mg^{-1}_{cat.}$	6.78	22
γ-Fe_2O_3	0.1 M KOH	0.212 μg h^{-1} $mg^{-1}_{cat.}$	1.9	23
Fe_3O_4/Ti	0.1 M Na_2SO_4	3.42 μg h^{-1} cm^{-2}	2.6	24
Fe_2O_3-CNT	$KHCO_3$	0.22 μg h^{-1} cm^{-2}	0.15	25
Mo nanofilm	0.01 M H_2SO_4	1.89 μg h^{-1} cm^{-2}	0.72	26
MoS_2/CC	0.1 M Na_2SO_4	4.94 μg h^{-1} cm^{-2}	1.17	11
Fe-N/C-CNTs	0.1 M KOH	34.83 μg h^{-1} $mg^{-1}_{cat.}$	9.28	27
MoN	0.1 M HCl	18.42 μg h^{-1} cm^{-2}	1.15	28
PEBCD/C	0.5 M Li_2SO_4	1.58 μg h^{-1} cm^{-2}	2.85	29
N-doped porous carbon	0.05 M H_2SO_4	23.8 μg h^{-1} $mg^{-1}_{cat.}$	1.42	30

Table S2. Data obtained from the ion chromatography for NH^{4+} concentrations after electrolysis for 2h at a series of potentials.

Sample	Potential (V vs. RHE)	Concentration (NH_4^+, mg L^{-1})
1	–0.35	0.0152
2	–0.4	0.0464
3	–0.45	0.1431
4	–0.5	0.1024
5	–0.6	0.1009

References

1. D. Zhu, L. Zhang, R. E. Ruther and R. J. *Hamers*, *Nat. Mater.,* 2013, **12**, 836–841.
2. G. W. Watt and J. D. Chrisp, *Anal. Chem.,* 1952, **24**, 2006–2008.
3. G. Kresse and J. Furthmuller, *Phys. Rev. B: Condens. Matter Mater. Phys.*, 1996, **54**, 11169−11186.
4. G. Kresse and J. Furthmuller, *Comput. Mater. Sci.*, 1996, **6**, 15−50.
5. P. E. Blöchl, *Phys. Rev. B: Condens. Matter Mater. Phys.,* 1994, **50**, 17953−17979.
6. J. P. Perdew, K. Burke and M. Ernzerhof, *Phys. Rev. Lett.,* 1996, **77**, 3865−3868.
7. M. Guo, Y. Yang, Y. Leng, L. Wang, H. Dong, H. Liu and W. Li, *J. Mater. Chem. C*, 2017, **5**, 4845−4851.
8. X. Li, S. Guo, W. Li, X. Ren, J. Su, Q. Song, A. J. Sobrido and B. Wei, *Nano Energy*, 2019, **57**, 388−397.
9. W. Hu, T. Wang, R. Zhang and J. Yang, *J. Mater. Chem. C*, 2016, **4**, 1776−1781.
10. X. Liu and Z. Li, *J. Phys. Chem. Lett.*, 2015, **6**, 3269−3275.
11. L. Zhang, X. Ji, X. Ren, Y. Ma, X. Shi, Z. Tian, A. M. Asiri, L. Chen, B. Tang and X. Sun, *Adv. Mater.,* 2018, **30,** 1800191.
12. S. Grimme, *J. Comput. Chem.,* 2006, **27**, 1787−1799.
13. D. R. Lide, Ed. CRC Handbook of Chemistry and Physics, 85th ed.; CRC Press: Boca Raton, FL, 2004.
14. M. Shi, D. Bao, S. Li, B. Wulan, J. Yan and Q. Jiang, *Adv. Energy Mater.,* 2018, **8**, 1800124.
15. D. Bao, Q. Zhang, F. Meng, H. Zhong, M. Shi, Y. Zhang, J. Yan, Q. Jiang and X. Zhang, *Adv. Mater.,* 2017, **29**, 1604799.
16. M. Nazemia, S. R. Panikkanvalappila and M. A. E. Sayed, *Nano Energy,* 2018, **49**, 316–323.

17. H. Huang, L. Xia, X. Shi, A. M. Asiri, and X. Sun, *Chem. Commun.,* 2018, **54**, 11427–11430.
18. H. Liu, S. Han, Y. Zhao, Y. Zhu, X. Tian, J. Zeng, J. Jiang, B. Xia and Y. Chen, *J. Mater. Chem. A,* 2018, **6**, 3211–3217.
19. W. Fu, Y. Cao, Q. Feng, W. R. Smith, P. Dong, M. Ye* and J. Shen, *Nanoscale,* 2019, DOI:10.1039/C8NR08724E.
20. J. Wang, L. Yu, L. Hu, G. Chen, H. Xin and X. Feng, *Nat. Commun.,* 2018, **9**, 1795.
21. C. Lv, C. Yan, G. Chen, Y. Ding, J. Sun, Y. Zhou and G. Yu, *Angew. Chem., Int. Ed.,* 2018, **57,** 6073–6076.
22. Y. Zhang, W. Qiu, Y. Ma, Y. Luo, Z. Tian, G. Cui, F. Xie, L. Chen, T. Li, and X. Sun, *ACS Catal.,* 2018, **8**, 8540–8544.
23. J. Kong, A. Lim, C. Yoon, J. H. Jang, H. C. Ham, J. Han, S. Nam, D. Kim, Y. E. Sung, J. Choi and H. S. Park, *ACS Sustain. Chem. Eng.,* 2017, **5**, 10986–10995.
24. Q. Liu, X. Zhang, B. Zhang, Y. Luo, G. Cui, F. Xie, and X. Sun, *Nanoscale,* 2018, **10**, 14386–14389.
25. S. Chen, S. Perathoner, C. Ampelli, C. Mebrahtu, D. Su and G. Centi, *Angew. Chem., Int. Ed.,* 2017, **56,** 2699–2703.
26. D. Yang, T. Chen and Z. Wang, *J. Mater. Chem. A,* 2017, **5,** 18967–18971.
27. Y. Wang, X. Cui , J. Zhao , G. Jia, L. Gu, Q. Zhang, L. Meng, Z. Shi, L. Zheng, C. Wang, Z. Zhang, and W. Zheng, *ACS Catal.,* 2019, **9**, 336-344.
28. L. Zhang, X. Ji, X. Ren, Y. Luo, X. Shi, A. M. Asiri, B. Zheng, and X. Sun, *ACS Sustainable Chem. Eng.,* 2018, **6**, 9550–9554.
29. G. Chen, X. Cao, S. Wu, X. Zeng, L. Ding, M. Zhu and H. Wang, *J. Am. Chem. Soc.,* 2017, **139**, 9771–9774.
30. Y. Liu, Y. Su, X. Quan, X. Fan, S. Chen, H. Yu, H. Zhao, Y. Zhang and J. Zhao, *ACS Catal.,* 2018, **8,** 1186−1191.